A Fully-Printed Self-Biased Polymeric Audio Amplifier for Driving Fully-Printed Piezoelectric Loudspeakers

Bahman Kheradmand-Boroujeni, Georg Cornelius Schmidt, Daniel Höft, Maxi Bellmann, Katherina Haase, Koichi Ishida, *Member, IEEE*, Reza Shabanpour, Tilo Meister, *Member, IEEE*, Corrado Carta, *Member, IEEE*, Pol Ghesquiere, Arved C. Hübler, and Frank Ellinger, *Senior Member, IEEE*

***Abstract*—In this paper, a printed audio amplifier, which is a new application for organic electronics, is suggested. The amplifier consists of several fully-printed bendable components including: a loudspeaker, organic field effect transistors (OFETs), capacitors, and resistors. All components are fabricated on polyethylene terephthalate (PET) substrate by means of high-throughput printing techniques. A complete self-biased circuit is reported consisting of large multi-finger OFETs with channel length of 20 μm and total width of 0.475 meter. The amplifier provides a peak voltage gain of 18 dB at 400 Hz, can reproduce sound pressure level of 36–60 dBA over 700 Hz to 12.5 kHz at one meter distance, and has a unity-gain-bandwidth of 17.7 kHz/5.2 kHz when driving 0 nF/$\sim$39 nF load at $V_{DD} = 80$ V, respectively. The impact of bias-stress effects on the amplifier performance is measured to be $\sim$3 dBA sound loss after 5 hours of continuous operation. The whole circuit is packaged and laminated on a separate PET sheet. In addition, the intrinsic electrical impedance of the printed PVDF-TrFE piezoelectric polymer used in the loudspeaker is characterized, and is modeled by a complex dielectric constant.**

***Index Terms*—Amplifiers, analog circuits, audio systems, flexible printed circuits, loudspeakers, OFETs, organic thin film transistors, polymer films.**

I. Introduction

PRINTED electronics is mainly intended for the low-cost mass production of large-area components on flexible plastic substrate [1]. In this regard, several applications such as: 1) flexible displays [2]; 2) RFID tags [3]; 3) ambient light sensors [4], etc., have been so far investigated.

In addition, the softness of polymeric materials used in printed electronics could make this technology also suitable for bioelectronics applications, because a flexible organic transistor can make a reliable and stable contact with an arbitrary shape biological system [5]. For example, printed organic transistors

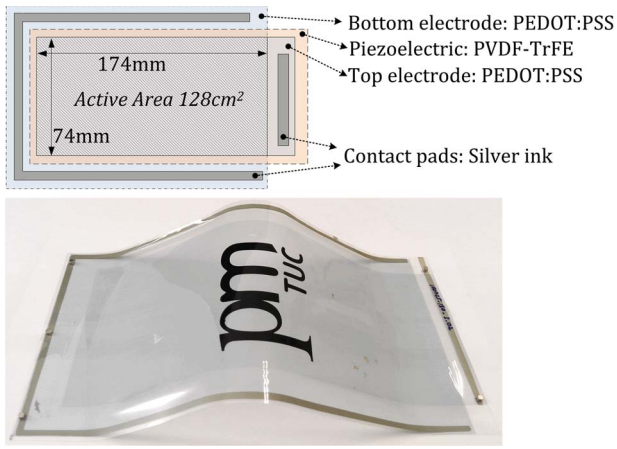

Fig. 1. Fully mass printed piezoelectric loudspeaker on plastic substrate. Structure and photograph of the loudspeaker used in this work.

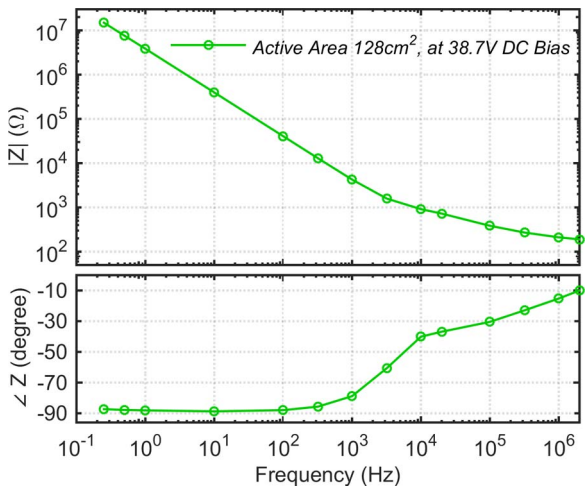

Fig. 2. Electrical impedance of the printed piezoelectric loudspeaker used in this work.

Manuscript received November 20, 2015; revised January 20, 2016; accepted February 12, 2016. This work was supported in part by the European Commission under the Flexible Multifunctional Bendable Integrated Light-weight Ultrathin Systems (FLEXIBILITY) project, and in part by the Organic/Polymer Path of Center for Advancing Electronics Dresden (cfaed), and in part by the DFG project Low-Voltage High-Frequency Vertical Organic Transistors (HFOE). This paper was recommended by Associate Editor K.-H. Chen.

B. Kheradmand-Boroujeni, K. Ishida, R. Shabanpour, T. Meister, C. Carta, and F. Ellinger are with the Chair for Circuit Design and Network Theory, Technische Universität Dresden, 01062 Dresden, Germany (e-mail: bahman.kheradmand_boroujeni@tu-dresden.de; koichi.ishida@tu-dresden.de; reza.shabanpour@tu-dresden.de; tilo.meister@tu-dresden.de; corrado.carta@tu-dresden.de; frank.ellinger@tu-dresden.de).

G. C. Schmidt, D. Höft, M. Bellmann, K. Haase, and A. C. Hübler are with the Institute for Print and Media Technology, Chemnitz University of Technology, 09126 Chemnitz, Germany (e-mail: georg.schmidt@mb.tu-chemnitz.de; hoeft.daniel@googlemail.com; maxi.bellmann@mb.tu-chemnitz.de; katherina.haase@gmail.com; arved.huebler@mb.tu-chemnitz.de).

P. Ghesquiere is with the Corporate Technology Department of Siemens, Siemens AG, 81739 Munich, Germany (e-mail: pol.ghesquiere@siemens.com).

Color versions of one or more of the figures in this paper are available online at http://ieeexplore.ieee.org.

Digital Object Identifier 10.1109/TCSI.2016.2538060

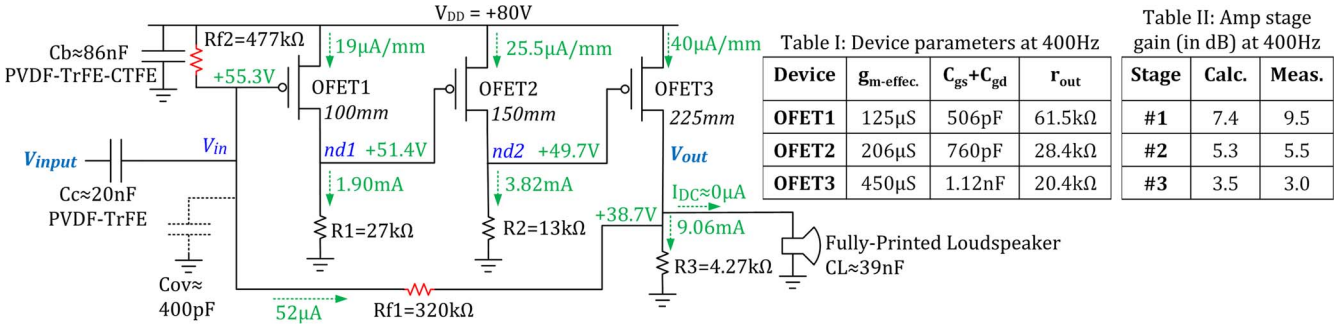

Table I: Device parameters at 400Hz

Device	$g_{m\text{-effec.}}$	$C_{gs}+C_{gd}$	r_{out}
OFET1	125µS	506pF	61.5kΩ
OFET2	206µS	760pF	28.4kΩ
OFET3	450µS	1.12nF	20.4kΩ

Table II: Amp stage gain (in dB) at 400Hz

Stage	Calc.	Meas.
#1	7.4	9.5
#2	5.3	5.5
#3	3.5	3.0

Fig. 3. Schematic of the fully-printed audio amplifier, dc bias points, OFET small-signal parameters, and calculated/measured amplifier stage gains at 400 Hz.

on a 1-μm-thick polymer film for on-body sensors are demonstrated in [6], and it is shown that printed differential amplifiers can be used for immunoglobulin G biosensors [7]. Also, a printed time-temperature dose recording tag for monitoring the spoilage of perishable products, e.g., food, is reported in [8].

Several reports on circuit design with organic technologies have been recently published. A 240-stage shift-register is reported in [9]. Many logic circuits such as D flip-flop, latch, and counter are implemented in [3]. An operational transconductance amplifier with 60 dB dc gain and 57 Hz gain-bandwidth-product, for measuring the current of an organic photodiodes, is reported in [4]. Printed half-wave and full-wave rectifiers [10] as well as a charge pump voltage multiplier [11] based on organic diodes are demonstrated. In [12], a 4-bit counting ADC with a sample rate of $\sim$4 Hz is reported. In [13], an AM demodulator with clock/data frequencies of 10 kHz/10 Hz is presented. A screen-printed 7-stage oscillator is reported in [14], which oscillates at 186 Hz. A folded-cascode amplifier with 40 dB low-frequency gain and a unity-gain-bandwidth of 1.5 kHz is demonstrated in [15] and has been employed in a switched-capacitor comparator.

However, most of the above-mentioned circuits are not fabricated solely using printing techniques. For example, the technologies used in [3], [4], [12]–[15] use gold sputtering and laser ablation for forming the source and drain electrodes and defining the channel. Thermal evaporation through a shadow mask has been used in [10]; and photolithography has been used in [9]. In [6] and [8], the dielectric layer is spin coated. In [7], the semiconductor layer is drop-casted, and the dielectric layer is also not printed.

Two fully-additively printed amplifiers have been reported in [16] and [17], showing 7–27 dB gain at low-frequencies, and 50–70 Hz unity-gain-bandwidth.

An important missing part in most of the previously reported analog organic circuits is the bias circuitry. Although biasing is also a key part of analog silicon circuits, it becomes more important and challenging in printed technologies because of the higher process variations, and bias-stress effect in these transistors which can dynamically change the device threshold voltage and I–V characteristics. For example, the amplifiers reported in [4], [7], [14]–[17] and the comparators in [13] have been biased using external voltage and current sources. Few circuit techniques have been proposed so far for addressing these biasing challenges in organic technologies. For example, common-mode feedback has been utilized in [18] to reduce the sensitivity of single-stage differential amplifiers to threshold voltage variations.

In a previous work, we have demonstrated the first fully mass printed, polymeric, piezoelectric loudspeaker on paper and polyethylene terephthalate (PET) substrate [19]. In another work [20], we have demonstrated a truly fully-printed, all-polymer, three-layer-dielectric (3L) organic field effect transistor (OFET) technology on flexible PET substrate, but only a ring oscillator circuit was demonstrated in that paper, which could generate a single tone beep with the loudspeaker.

The speaker used in this work is illustrated in Fig. 1. It has an active area of 128 cm^2 and a capacitor-like structure. PEDOT:PSS top/bottom conductive electrodes, $\sim$30 μm active layer of piezo-polymer poly(vinylidene fluoride-trifluorethylene) (PVDF-TrFE), and silver contact pads are all fabricated via sheet-fed screen printing.

The electrical impedance of the speaker is shown in Fig. 2. Below 1 kHz, the device behaves like a $\sim$39 nF capacitor, which is quite a heavy load. Above 1 kHz, the quality factor $Q = -\tan(\angle \mathrm{Z})$ starts to decrease, mainly because of the parasitic top/bottom electrode sheet resistances.

In Section II, we present the designed audio amplifier, and its electrical and acoustical measurement results. Detailed analyses of the piezo-polymer electrical impedance, its voltage linearity, and energy conversion efficiency are discussed in Section III. Methods for lowering the high operation voltage of the speaker and the OFET are discussed in Section IV.

II. Fully-Printed Self-Biased Audio Amplifier

Even so our printing technology has been recently significantly improved, it is still not mature enough and there are many issues which impose limitations on the circuit design side. For example, the yield concerns such as short circuits between the source (S) and drain (D) fingers, or gate (G) to S/D shorts through the pinholes in the dielectric, limit the number and size of the OFETs in a circuit. Also, the limited number of interconnection layers restricts the circuit complexity and even the number of resistors and capacitors which can be used in the circuit. In addition, the large V_{SD} bias needed across an OFET for keeping it in the saturation region, makes stacking and cascoding techniques impractical with a reasonable supply voltage. Keeping all these limitations in mind, we designed the self-biased, three-stage amplifier shown in Fig. 3 with only three OFETs.

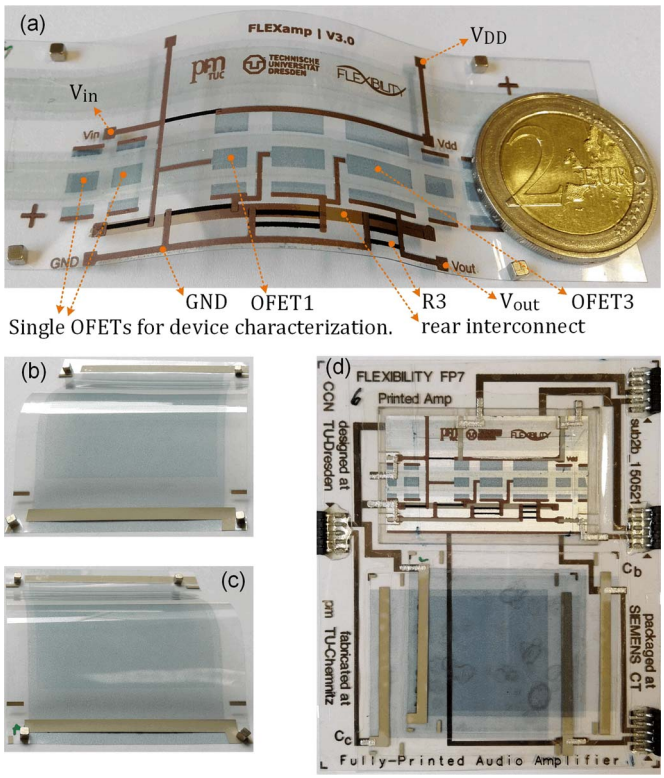

Fig. 4. Photographs of the fully-printed components. (a) OFETs and resistors. (b) PVDF-TrFE coupling capacitor. (c) PVDF-TrFE-CTFE bypass capacitor. (d) Complete amplifier after encapsulation and packaging.

The all-polymer, top-gate bottom-contact OFETs are fully printed onto a 100-μm-thick flexible PET substrate shown in Fig. 4(a). First, PEDOT:PSS source/drain electrodes are printed by the Cyflex technology at a printing speed of 0.3 m/s. Then, a blend of the small molecule CP-DIPS pentacene semiconductor and amorphous PTAA is gravure printed. For the dielectric, a stack of $\sim$325 nm CYTOP as a low-k for a good interface, $\sim$100 nm PVA modified with a fluorosurfactant as intermediate layer, and $\sim$1.35 μm ter-polymer poly[(vinylidenefluoride-co-trifluoroethylen-chlorotrifluoroethylen] (P(VDF-TrFE-CTFE)) as a high-k layer are printed. Finally, another PEDOT:PSS ink is screen printed for the gate electrode and S/D contact pads. Details of the technology and typical I–V curves can be found in [20].

Two different carbon particle based ink formulations with adapted conductivity of 790 S/cm and 50 S/cm are used for the resistors R1, 2, 3, and Rf1, 2 to keep the printing area small. This means, for Rf1, 2 a printing ink with high sheet resistance is selected. In contrast, for R1, 2, 3 an ink with much lower sheet resistance is used. Both inks are screen printed.

PEDOT:PSS ink used for the G/S/D electrodes results in a low gate leakage and a semi-transparent OFET, but this conductive conjugated polymer is too ohmic for long interconnections. Therefore, interconnects are flexo-printed with a silver coated copper particle ink. One interconnect, which connects $V_{\rm out}$ to Rf1, is printed on the rear of the substrate and is connected to the front by vias. The vias are realized with laser drilling, and are filled with the conductive ink during the flexo printing process.

A. Electrical and Acoustical Performances

The measured dc bias points and resistor values are given in Fig. 3. The expected small-signal parameters given in the inset Table I are extracted by measuring single OFETs shown in Fig. 4(a) using characterization techniques reported in [21]. The effective transconductance $(g_{m-\rm effec.})$, and the output resistance $(r_{\rm out})$ include the impact of parasitic S/D finger resistances. The low-frequency stage gains can then be easily calculated, and are compared to the measured values in the inset Table II. The measured gains are within -0.5 dB to $+2.1$ dB of the expected values. This proves acceptable uniformity and no short circuits along the substrate.

In the amplifier, R1, 2, 3 are decreased in a way that the current density, i.e., $\rm I_D/W$, increases from 19 μA/mm (per millimeter width) in OFET1 to 40 μA/mm in OFET3, resulting in $V_{\rm SG1} < V_{\rm SG2} < V_{\rm SG3}$, which would then result in a positive $V_{\rm GD1}$ and $V_{\rm GD2}$. The feedback resistors Rf1, 2 bias $\rm V_{out}$ node well below $nd2$, to maximize the output swing.

A normal human voice has a low energy content above 10 kHz. On the other side, the speaker performance becomes weak below 300 Hz, which means that the amplifier performance below 300 Hz is also not important. Although this slightly relaxes the requirements on the input coupling components Cc and Rf1, 2, still large R–C time constant would be needed at the amplifier input for passing signals above 300 Hz. In addition, a high gate leakage in OFET1, or a high dielectric leakage through Cc, would directly affect the bias $\rm V_{out}$ voltage. Therefore we used a low-leakage dielectric for the fully-printed coupling capacitor Cc, but a high-k dielectric for the bypass capacitor Cb as explained in Section II-C. The capacitor photos are shown in Fig. 1(b) and (c).

The amplifier frequency response is shown in Fig. 5. $\rm V_{in}$, $nd1$, and $nd2$ are only measured for the loaded amplifier (i.e., with loudspeaker), but $\rm V_{out}$ is measured for both loaded and unloaded cases. The amplifier shows $\sim$18 dB peak gain at 400 Hz, and a unity-gain-bandwidth of 5.3 kHz/17.7 kHz for loaded/unloaded cases, respectively. An example of the voltage waveforms is shown in Fig. 6, reaching 16 $V_{\rm pp}$ output swing. For better visibility, only the ac-coupled output voltage is shown in this figure. The dc level of $V_{\rm out}$ in given in Fig. 3 and has almost no impact on the output sound. The output swing is mainly limited by the OFET2, 3 nonlinearities, because the swing at $nd1$ is much smaller than $nd2$ and $\rm V_{out}$.

Fig. 7 shows the sound pressure level (SPL), at one meter distance, with a 0.8 $\rm V_{rms}$ input signal to the amplifier, measured in an anechoic chamber. All acoustic measurements are performed using the acoustic measurement system Apollo from SINUS. The SPL fluctuations in the frequency response are given by the acoustical properties of the speaker especially its shape and size as explained in [19]. As we can see in Figs. 2 and 5, the speaker impedance and the amplifier frequency response change quite smoothly with frequency. For example from 11 kHz to 16 kHz, the amplifier voltage gain decreases 4.6 dB, but the output sound decreases 23.3 dBA, i.e., 18.7 dBA loss is from the speaker. However, 3.4 dB of this amount is from the attenuation in the A-weight filtering used in the measurement system. This filtering relates to the human ear frequency response and attenuates very low and very high frequencies which are difficult to

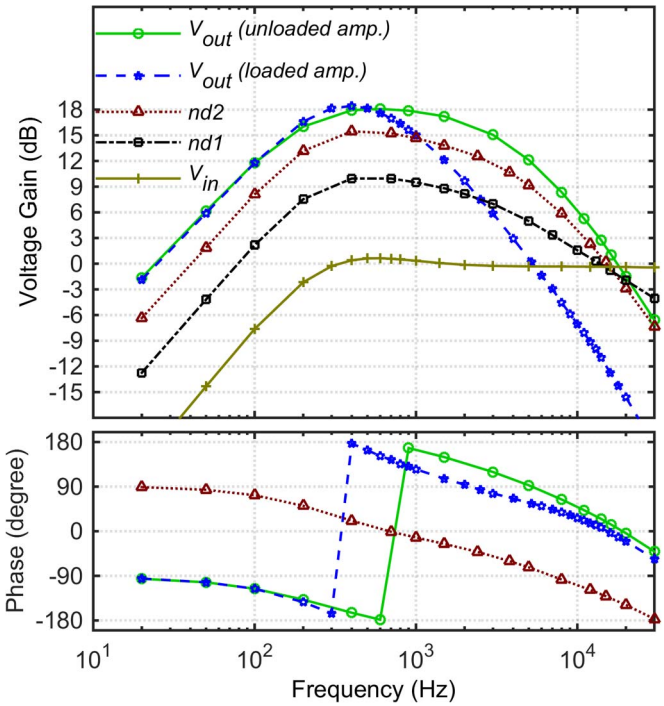

Fig. 5. Frequency response of the amplifier, when driving the loudspeaker (loaded), and not driving the loudspeaker (unloaded), at $V_{DD} = 80$ V, 25 °C.

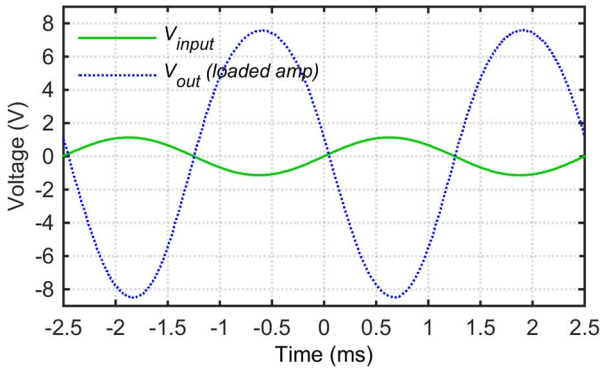

Fig. 6. Input and ac output waveforms at 400 Hz, $V_{input} = 800$ mV_{rms}, $V_{DD} = 80$ V, 25 °C.

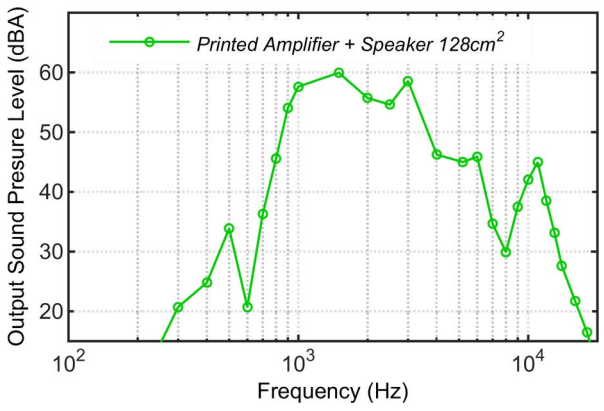

Fig. 7. Acoustic output of the audio amplifier at 1 m distance above the loudspeaker, with $V_{input} = 800$ mV_{rms} sinus signal, at $V_{DD} = 80$ V, 25 °C.

hear. Therefore, the real performance loss of the speaker from 11 kHz to 16 kHz is 15.3 dB. As we will see in Section III, the sound pressure is linearly proportional to the voltage applied into the speaker.

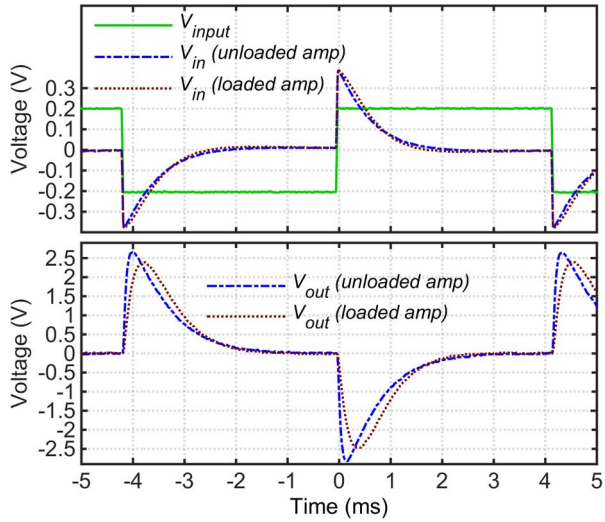

Fig. 8. Small-signal step response of the amplifier, showing no ringing and good stability, at $V_{DD} = 80$ V, 25 °C.

The output SPL is within 36–60 dBA over 700 Hz to 12.5 kHz at 1 m distance. Although it is not a strong sound, when applying a ∼800 mV_{rms} music signal to the amplifier, under quiet condition it is audible by young people up to ∼5 m distance.

The feedback resistors Rf1, 2 are only intended for biasing the amplifier. As we can see in Fig. 5, above 300 Hz, V_{in} is fully shorted to V_{input} and Rf1, 2 become a negligible load at the input and output nodes. However, since they create a feedback loop, the stability should be checked. Fig. 8 shows small-signal step responses of the amplifier, clearly showing no ringing for both loaded and unloaded cases. From the phase data in Fig. 5, e.g., for the loaded case, we have 90° phase delay and 8.8 dB gain at 2.17 kHz from V_{in} to V_{out}. Since Cc is much larger than the OFET1 gate capacitance given in the inset Table I in Fig. 3, we can assume a simple R–C filter from V_{out} to V_{in}, with additional ∼90° phase delay and 38.8 dB attenuation at 2.17 kHz; i.e., the loop has a gain margin of ∼30 dB. We could have further attenuation in the R–C filter and therefore better loop stability by increasing the Cc and/or Rf1, 2. However, the gate leakages of OFET1 and Cc pose a maximum limit on Rf1, 2 values because these dc currents mainly pass through Rf1 and could change the bias of V_{out}.

In Fig. 8, we do not see a big difference between the loaded and unloaded cases. Also, in Fig. 5 the loaded and unloaded frequency responses are quite similar below 500 Hz. The parallel connection of the speaker with $R3 \| r_{out3}$ makes a pole at ∼1.2 kHz for the loaded case. Below this frequency, the input resistance at V_{in}, i.e., Rin, would be Rf2 in parallel with $Rf1/(1 + A_{v0})$ where A_{v0} is the inverting gain of the three-stage amplifier, i.e., $A_{v0} \approx 8$. The series connection of the coupling capacitor Cc with $Rin \| Cov \| C_{g-OFET1}$ makes a zero at 0 Hz and a pole at ∼230 Hz, independent of CL value.

Fig. 9 shows the impact of the supply voltage (V_{DD}) variation on the key circuit characteristics. Clearly, increasing the V_{DD} increases the current through the OFETs and therefore improves the g_m. As a result, gain and bandwidth of the amplifier improve with V_{DD}.

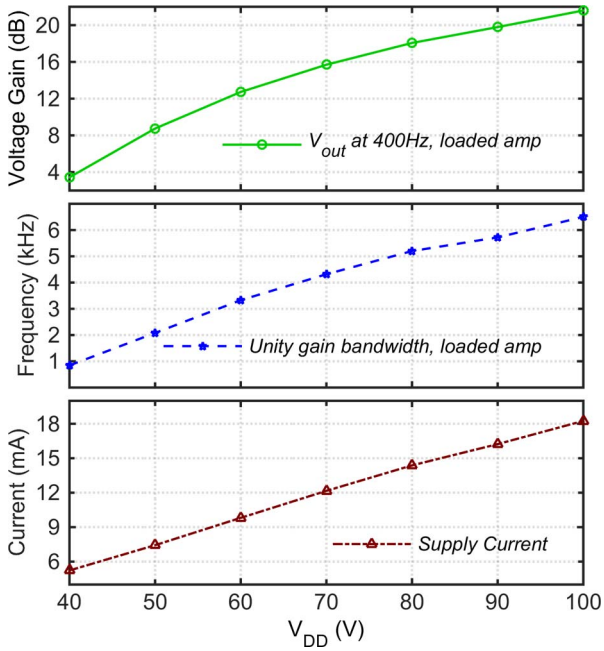

Fig. 9. Amplifier performance as a function of supply voltage, at 25 °C.

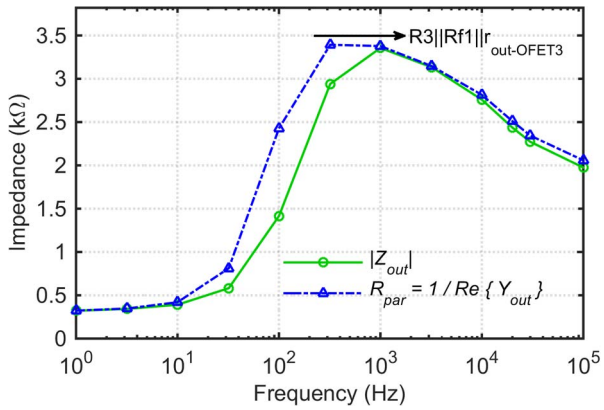

Fig. 10. Output impedance of the unloaded amplifier, at $V_{DD} = 80$ V, 25 °C.

The absolute value of the output impedance $|Z_{out}|$, and the parallel output resistance R_{par} calculated from the real part of the output admittance $Y_{out} = 1/Z_{out}$, of an unloaded amplifier, are shown in Fig. 10. At low frequencies below 300 Hz, the feedback loop significantly decreases the Z_{out}. The peak value of R_{par} is around $R3||Rf1||r_{out-OFET3}$ as expected. Since the printed OFET has quite large $C_{gd} \approx C_{gs}$, at high frequencies above ∼10 kHz, $C_{gd3} \approx 560$ pF provides ∼43% coupling from V_{out} to $nd2$, resulting in an additional parallel output resistance of $\sim 2.3/g_{m3}$. Also, the Q-factor of $C_{gs/d3}$ starts decreasing above 10 kHz, therefore R_{par} continue decreasing with frequency.

The OFET threshold voltage is ∼5 V, i.e., the drain voltage can go up to ∼5 V above the gate voltage. The voltage linearity of the amplifier is shown in Fig. 11. As expected, the maximum compression happens at 400 Hz where we have the maximum gain and voltage swing at $nd1$, $nd2$, and V_{out}. However, even with at 1 V_{rms} input, only 2.0 dB/1.6 dB/0.8 dB compression is observed at 400 Hz/1.6 kHz/3.1 kHz, respectively, which

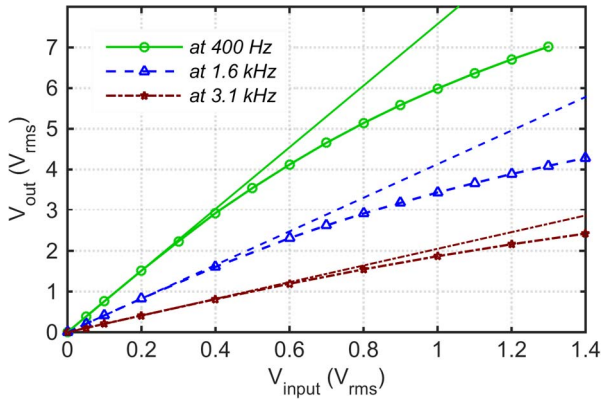

Fig. 11. Voltage linearity of the loaded amplifier, at $V_{DD} = 80$ V, 25 °C.

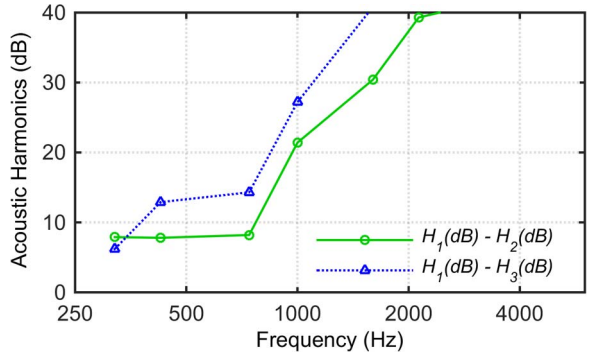

Fig. 12. Second and third harmonics of the output sound, relative to the first harmonic, at 1 m distance above the loudspeaker, $V_{input} = 800$ mV_{rms}, $V_{DD} = 80$ V, 25 °C.

are quite small comparing to the speaker's intrinsic SPL non-uniformities and fluctuations.

To further evaluate the output sound quality, the second and third harmonics of the output sound are measured using the acoustic measurement system Apollo with a 10 inch microphone. The results are shown in Fig. 12. Above 1 kHz, harmonics become more than 20 dB smaller than the main sound (i.e., H_1). The sound quality becomes low below 700 Hz because: a) the voltage linearity of the amplifier decreases; and b) harmonics are at two/three times higher frequencies, where the speaker is much more sensitive. The fourth and higher order harmonics are negligible.

B. Bias-Stress Effect

Charge trapping in non-single-crystalline semiconductive films, such as organic materials, causes device characteristics changes. Five-hour bias-stress tests on the 3L OFET are reported in [20]. Continuous five-hour bias-stress tests on the printed amplifier are shown in Fig. 13. Since the threshold voltage slowly increases with time, V_{SG1} increases and causes the reduction of V_{out} dc bias and the supply current. The $g_{m1,2,3}$ and therefore the amplifier performance degrade with time because of: a) reduction of the drain current in OFET1, 3; and b) reduction of the effective charge carrier mobility in all OFETs due to charge trapping. ∼3 dB gain loss is observed after five hours, which causes 3 dBA lower sound.

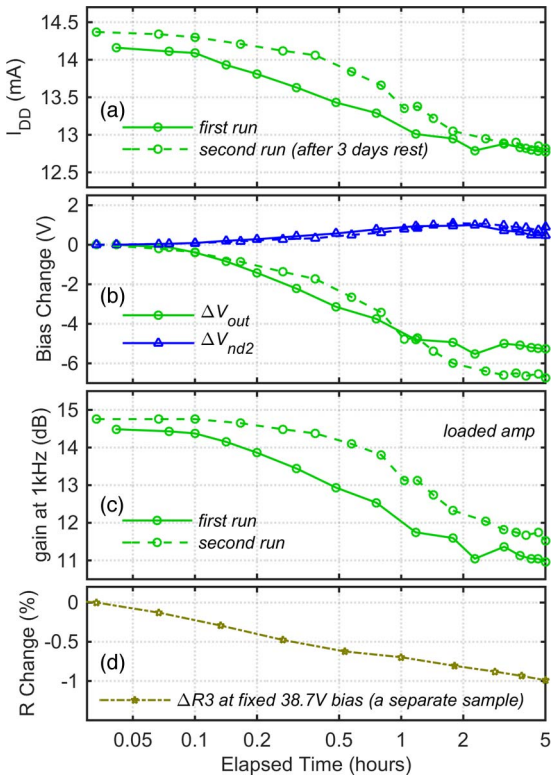

Fig. 13. Bias stress effects during five hours of continuous operation at $V_{DD} =$ 80 V, 25 °C. (a) Supply current change. (b) DC bias change at V_{out} and $nd2$ nodes. (c) Voltage gain change. (d) A separately measured single R3 resistor at fixed 38.7 V bias.

The five-hour test is repeated after letting the circuit to rest for three days. Quite similar results are obtained in the second run. This indicates that most of the trapped charges have been released, and the circuit has recovered during the rest period.

In order to check that the observed performance degradation is not caused by the resistors, an individual R3, which has the highest current density among all resistors, is printed on a separate substrate, and is biased at fixed 38.7 V using Agilent 2901A SMU for five hours as shown in Fig. 13(d). Only 1% resistance loss is observed, whereas 10% supply current reduction is observed in Fig. 13(a), which means that the impact of the bias-stress in OFETs on the amplifier performance is quite dominant. Since printed layers could be porous, probably joule heating in the resistor changes the morphology and decreases the resistance.

C. Fully-Printed Capacitors

As mentioned in Section II, quite large and high-voltage capacitors are needed in the circuit, e.g., for feeding low audio frequencies into the amplifier through the coupling capacitor Cc. We screen printed two types of capacitors, one with the high-k PVDF-TrFE-CTFE dielectric for the bypass capacitor Cb, and the other one with PVDF-TrFE dielectric for Cc, both have 16 cm^2 active area, and PEDOT:PSS top/bottom electrodes as illustrated in Fig. 4(b) and (c). Contact pads are printed with silver ink.

The electrical impedance Z of capacitors is measured similar to the Cytop capacitors in [21]. Then C is calculated from the real part of the admittance $Y = 1/Z$, i.e., $C = \mathrm{Re}\{Y\}/\omega$,

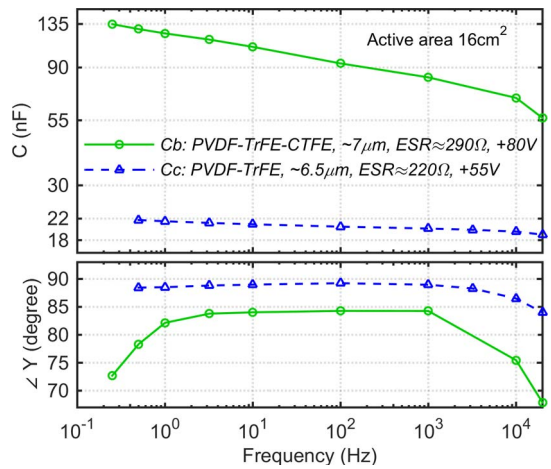

Fig. 14. Fully-printed coupling and bypass capacitors. Measured C and angle of admittance as a function of frequency at 25 °C.

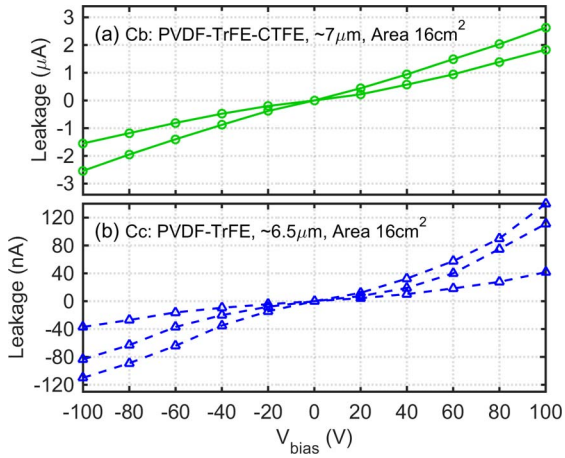

Fig. 15. Leakage current of printed capacitors as a function of applied voltage at 25 °C. (a) Two samples of the bypass capacitor. (b) Three samples of the coupling capacitor.

and is shown in Fig. 14. As expected, the high-k polymer provides much higher capacitance, but it is also more frequency dependent.

The dielectric leakage of multiple samples are compared in Fig. 15. Although PVDF-TrFE has 4.4 times lower dielectric constant at 1 kHz, it shows ∼32 times lower leakage at +55 V. Therefore, PVDF-TrFE is more suitable for the Cc while PVDF-TrFE-CTFE is more suitable for the Cb.

We have to mention that, although Cc has the same dielectric polymer as the printed speaker, it does not produce an audible sound. As we can see in Fig. 5, V_{in} is fully coupled to the V_{input} above 300 Hz, i.e., the ac voltage across the Cc becomes almost zero.

D. Encapsulation and Packaging

The complete module is shown in Fig. 4(d) and consists of a PET substrate equipped with the OFET substrate and the two capacitors. The printed OFET substrate [Fig. 4(a)] is laminated with a 200-μm-thick barrier foil, which significantly slows down the chemical degradation of OFETs caused by water/moisture and oxygen contamination. On the back side, a 35-μm-thick aluminum foil is taped for better heat distribution.

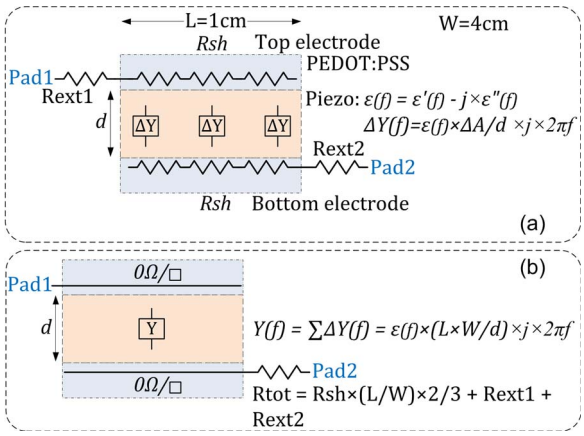

Fig. 16. Electrical impedance models of the printed symmetrical loudspeakers. (a) Distributed model. (b) Equivalent lumped form.

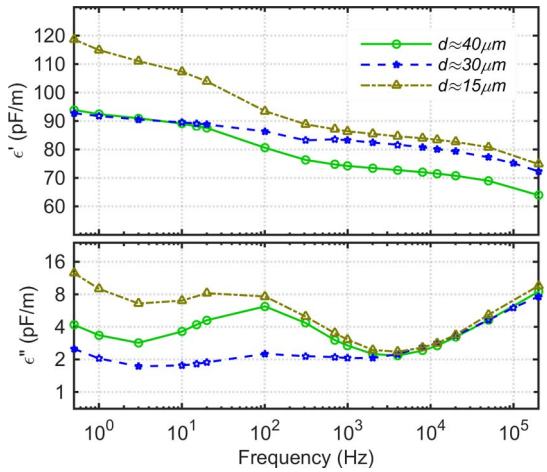

Fig. 17. Measured complex permittivity of printed PVDF-TrFE, at 25 °C.

To achieve highly conductive and homogenous interconnects, silver is inkjet-printed on another PET substrate and subsequently cured in a convection oven. After that, the OFETs and the capacitor Cc are attached face-up to the main substrate by means of a non-conductive adhesive foil. Due to space limitations, the two capacitors (Cb and Cc) are stacked upon each other. An adhesive foil is applied on the bottom side of capacitor Cb before assembly on the top side of capacitor Cc. This overlapping makes the parasitic capacitance Cov $\approx$ 400 pF shown in Fig. 3.

After that, a silver-based isotropic conductive adhesive is dispensed onto the connection pads of the components and the corresponding pads on the PET substrate. At the end, the complete module is protected against environmental influences and scratches by means of an additional 75-μm-thick barrier foil from 3M. We observed no damage to the circuit functionality after packaging.

III. Fully-Printed Piezoelectric Loudspeaker

Even non-printed piezoelectric polymers are known to have high dielectric and mechanical losses, elastic properties, and frequency-dependent dielectric constant with a complex part [22]. Therefore, advanced electromechanical models have been proposed for modeling them at MHz range [23].

A complex dielectric constant is expressed in the form of $\varepsilon = \varepsilon' - j \times \varepsilon''$, which results in an admittance $\mathrm{Y} = \mathrm{C} \times j\omega = (\varepsilon' - j \times \varepsilon'') \times (\mathrm{A/d}) \times j\omega$, where A is the area and d is the thickness of the dielectric layer. This gives a real part in Y, i.e., $\mathrm{Re}\{\mathrm{Y}\} = \varepsilon'' \times (\mathrm{A/d}) \times \omega$, which accounts for the real power consumption in the speaker.

To understand how much of the apparent power consumed by the speaker is transformed into other forms of energy (including sound), ε'' has to be measured. However, it is not possible to directly calculate the ε from a normal-size speaker impedance, because as we can see in Fig. 2, the high surface resistance of the PEDOT:PSS electrodes drastically affects the impedance above 1 kHz. To bypass this problem, we printed short-length, symmetrical speakers with structure shown in Fig. 16(a); i.e., with equal top and bottom electrode sheet resistances, and two similar contact pads on two opposite sides of the speaker (unlike the large speaker in Fig. 1 which one silver contact pad is printed on three sides to reduce the ESR). Under these criteria, even with a frequency-dependent $\varepsilon(f)$, the contribution of the PEDOT:PSS electrodes to the total impedance Z between $Pad1$ and $Pad2$ would be frequency-independent, and the structure shown in Fig. 16(a), would have equal impedance to the structure shown in Fig. 16(b), where Rsh is the sheet resistance of the electrodes, Rext1,2 are the resistance of the electrode extensions outside of the piezo area, L is the length and W is the width of the active piezo area. At very high frequencies, the impedance of the pure piezo layer in Fig. 16(b) becomes negligible comparing to the total electrode resistance Rtot; i.e., Rtot is measured from the real part of Z at MHz frequencies and is $\sim$270 Ω. Then, Rtot is subtracted from the Z, $\mathrm{Y} = 1/(\mathrm{Z\text{-}Rtot})$, and $\varepsilon'(f)$ and $\varepsilon''(f)$ are extracted from the Y and are shown in Fig. 17.

In order to verify the impedance equality of the distributed and lumped structures in Fig. 16, we divided the distributed network into 32 segments, and simulated both structures [i.e., Fig. 16(a) and (b)] in ADS with the complex ε obtained in Fig. 17, and observed that both real and imaginary parts are exactly equal. This confirms the correctness of our approach.

In Fig. 17, the measured ε is reported for three different piezo-polymer thicknesses. The ε'' is within 2.1–3.5 pF/m over the frequency range of 700 Hz–15 kHz where we have good acoustic performance in Fig. 7, whereas ε' is within 71–87 pF/m over the same range, since $\varepsilon''/\varepsilon'$ would be the ratio of real over reactive power, it is clear that most of the apparent power consumed by the speaker is just wasted in the capacitive part. On the other hand, the ε'' contains all forms of real energy consumptions in the speaker such as the output sound, dielectric loss, and mechanical vibration loss. It is not trivial to electrically measure each part separately. However, large SPL fluctuations are reported in [19] for different size speakers, and can be also seen in Fig. 7 e.g., within 8 kHz–13 kHz, whereas in Fig. 17 the ε'' changes very smoothly, without any sudden fluctuations. This suggests that the energy transformed into the sound is much smaller than the dielectric/mechanical losses.

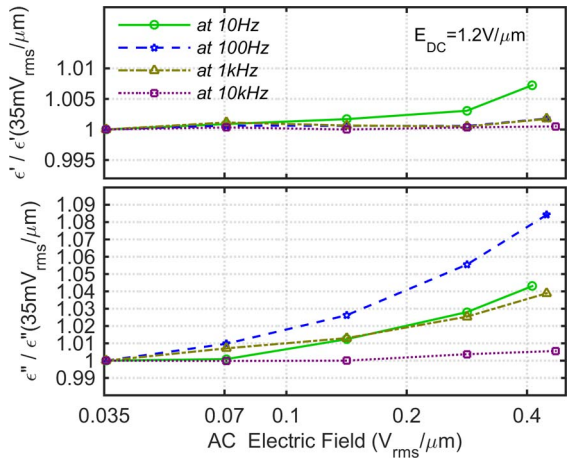

Fig. 18. Measured linearity of the complex permittivity of printed PVDF-TrFE as a function of applied ac electric field, at 25 °C.

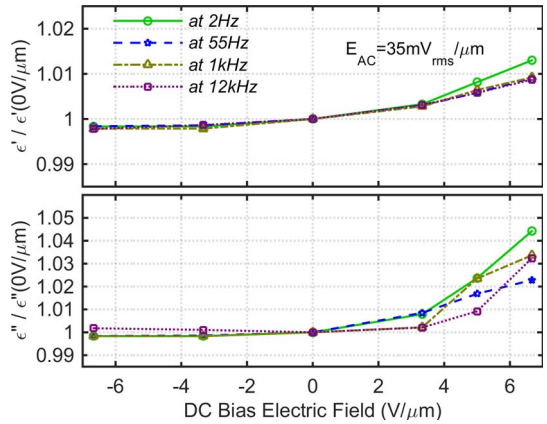

Fig. 19. Measured linearity of the complex permittivity of printed PVDF-TrFE as a function of applied dc electric field, at 25 °C.

The linearity of ε versus amplitude of the applied ac electric field, i.e., applied ac voltage divided by the piezo layer thickness, is shown in Fig. 18. The speaker is biased at the dc electric field of 1.2 V/μm, which is close to the dc bias point of the audio amplifier output at $\mathrm{V_{DD}} = 80$ V. The ε' is very constant, and the ε'' changes only $< 8\%$ up to 400 $\mathrm{mV_{rms}}/\mu$m. 16 Vpp output swing of the amplifier in Fig. 6 corresponds to $\sim$190 $\mathrm{mV_{rms}}/\mu$m. Similar results are shown in Fig. 19 versus the dc bias point of the speaker. The different behavior at positive and negative electric fields is because of the dielectric poling of the speaker. These results show that the speaker is biased and operates at a very linear and stable point from both ac and dc points of view. This is important because a nonlinear speaker impedance would result in additional voltage harmonics at $\mathrm{V_{out}}$ (because the amplifier has a relatively high output impedance) which would then further degrade the sound quality.

In addition, as shown in Fig. 20, we measured the output SPL as a function of applied ac voltage to the speaker at different frequencies. For this test, the speaker was driven by the power amplifier PA-1122 from Monacor, not by the printed circuit. A 20 dB/decade reference line is also drawn in this figure. Clearly, all SPL lines are parallel to the 20 dB/decade line, which means that the acoustic performance of the speaker has very good voltage linearity as well.

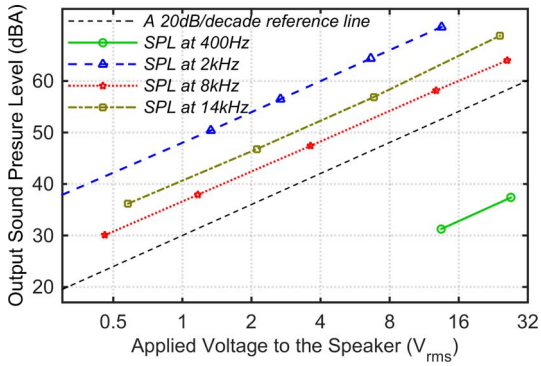

Fig. 20. Linearity of the output SPL as a function of applied voltage to the speaker, at 25 °C.

IV. Voltage Scalability

The $\mathrm{V_{DD}} = 80$ V is too high for some applications. However, several techniques can be used for reducing the required voltage of both speaker and amplifier in the future. For the OFETs, following techniques result in an equal $\mathrm{I_D}$ at lower voltage, and at the same time higher g_m at equal $\mathrm{I_D}$: a) printing thinner dielectric layers or using new dielectrics with higher ε_r; b) printing a shorter channel length; and c) using better polymer semiconductors with higher mobility. A higher g_m at equal $\mathrm{I_D}$ is also important because with a higher g_m the resistors R1, 2 3 and therefore the voltage across them can be decreased while having the same stage gain, i.e., $g_m \times$ R.

Regarding the speaker, it is known that its surface displacement is in the nanometer range [19]. The same electric field excitation can be created in the piezo layer at much lower voltage by printing a thinner piezo. However, this is at the moment challenging because of the large active area which has to be printed pinhole-free, to avoid shorts between the electrodes; and would also need a lighter (e.g., thinner) substrate. In addition, since the speaker has good voltage linearity, the sound can be considerably increased, or equivalently the $\mathrm{V_{DD}}$ can be further decreased, using a rail-to-rail differential output stage. However, this would require a complementary technology with both n- and p-type transistors. In order to significantly reduce the power consumption, one may design an inductor-based switching driver, which could recycle energy from the capacitive part of the speaker impedance. However, this would first require MHz transistors.

V. Conclusion

This work studied fully-printed audio systems as a new application for printed electronics on plastic. Clearly audible, although not very loud, sound is reproduced using all-polymer transistors and a piezo-polymer speaker. Promising results are obtained. To the best knowledge of the authors, this is the first fully-printed audio system capable of reproducing human voice and music. By further improvement of the technology, it will be possible to significantly reduce the supply voltage and power consumption, and improve the amplifier bandwidth. Talking books, advertisements or newsletters, and toys could be suitable market applications for this low-cost technology.

REFERENCES

[1] H. Marien, M. S. J. Steyaert, E. van Veenendaal, and P. L. Heremans, "On the other applications of organic electronics on foil," *IEEE Solid-State Circuits Mag.*, vol. 4, no. 4, pp. 43–49, Dec. 2012.

[2] M. Mizukami, S. Oku, S. Cho, M. Tatetsu, M. Abiko, M. Mamada, T. Sakanoue, Y. Suzuri, J. Kido, and S. Tokito, "A solution-processed organic thin-film transistor backplane for flexible multiphoton emission organic light-emitting diode displays," *IEEE Electron Device Lett.*, vol. 36, no. 8, pp. 841–843, Aug. 2015.

[3] V. Fiore, P. Battiato, S. Abdinia, S. Jacobs, I. Chartier, R. Coppard, G. Klink, E. Cantatore, E. Ragonese, and G. Palmisano, "An integrated 13.56-MHz RFID tag in a printed organic complementary TFT technology on flexible substrate," *IEEE Trans. Circuits Syst. I, Reg. Papers*, vol. 62, no. 6, pp. 1668–1677, Jun. 2015.

[4] G. Maiellaro, E. Ragonese, R. Gwoziecki, S. Jacobs, N. Marjanović, M. Chrapa, J. Schleuniger, and G. Palmisano, "Ambient light organic sensor in a printed complementary organic TFT technology on flexible plastic foil," *IEEE Trans. Circuits Syst. I, Reg. Papers*, vol. 61, no. 4, pp. 1036–1043, Apr. 2014.

[5] C. Liao, M. Zhang, M. Y. Yao, T. Hua, L. Li, and F. Yan, "Flexible organic electronics in biology: Materials and devices," *Adv. Mater.*, Nov. 2014, DOI: 10.1002/adma.201402625.

[6] K. Fukuda, Y. Takeda, Y. Yoshimura, R. Shiwaku, L. T. Tran, T. Sekine, M. Mizukami, D. Kumaki, and S. Tokito, "Fully-printed high-performance organic thin-film transistors and circuitry on one-micron-thick polymer films," *Nature Commun.*, vol. 5, Jun. 2014, Art. no. 4147.

[7] K. Fukuda, T. Minamiki, T. Minami, M. Watanabe, T. Fukuda, D. Kumaki, and S. Tokito, "Printed organic transistors with uniform electrical performance and their application to amplifiers in biosensors," *Adv. Electron. Mater.*, vol. 1, no. 7, Jul. 2015.

[8] T. N. Ng, D. E. Schwartz, P. Mei, B. Krusor, S. Kor, J. Veres, P. Bröms, T. Eriksson, Y. Wang, O. Hagel, and C. Karlsson, "Printed dose-recording tag based on organic complementary circuits and ferroelectric nonvolatile memories," *Nature Sci. Rep.*, vol. 5, Aug. 2015, Art. no. 13457.

[9] D. Raiteri, P. v. Lieshout, A. v. Roermund, and E. Cantatore, "Positive-feedback level shifter logic for large-area electronics," *IEEE J. Solid-State Circuits*, vol. 49, no. 2, pp. 524–535, Feb. 2014.

[10] P. S. Heljo, M. Li, K. E. Lilja, H. S. Majumdar, and D. Lupo, "Printed half-wave and full-wave rectifier circuits based on organic diodes," *IEEE Trans. Electron Devices*, vol. 60, no. 2, pp. 870–874, Feb. 2013.

[11] P. Heljo, K. E. Lilja, H. S. Majumdar, and D. Lupo, "High rectifier output voltages with printed organic charge pump circuit," *Organic Electron.*, vol. 15, no. 1, pp. 306–310, Jan. 2014.

[12] S. Abdinia, M. Benwadih, R. Coppard, S. Jacob, G. Maiellaro, G. Palmisano, M. Rizzo, A. Scuderi, F. Tramontana, A. van Roermund, and E. Cantatore, "A 4 b ADC manufactured in a fully-printed organic complementary technology including resistors," in *IEEE Int. Solid-State Circuits Conf. Dig. Tech. Papers (ISSCC)*, Feb. 2013, pp. 106–107.

[13] S. Abdinia, F. Torricelli, G. Maiellaro, R. Coppard, A. Daami, S. Jacob, L. Mariucci, G. Palmisano, E. Ragonese, F. Tramontana, A. H. M. van Roermund, and E. Cantatore, "Variation-based design of an AM demodulator in a printed complementary organic technology," *Organic Electron.*, vol. 15, no. 4, pp. 904–912, Apr. 2014.

[14] M. Guerin, A. Daami, S. Jacob, E. Bergeret, E. Benevent, P. Pannier, and R. Coppard, "High-gain fully printed organic complementary circuits on flexible plastic foils," *IEEE Trans. Electron Devices*, vol. 58, no. 10, pp. 3587–3593, Oct. 2011.

[15] G. Maiellaro, E. Ragonese, A. Castorina, S. Jacob, M. Benwadih, R. Coppard, E. Cantatore, and G. Palmisano, "High-gain operational transconductance amplifiers in a printed complementary organic TFT technology on flexible foil," *IEEE Trans. Circuits Syst. I, Reg. Papers*, vol. 60, no. 12, pp. 3117–3125, Dec. 2013.

[16] J. Chang, X. Zhang, T. Ge, and J. Zhou, "Fully printed electronics on flexible substrates: High gain amplifiers and DAC," *Organic Electron.*, vol. 15, no. 3, pp. 701–710, Mar. 2014.

[17] X. Zhang, T. Ge, and J. S. Chang, "Fully-additive printed electronics: Transistor model, process variation and fundamental circuit designs," *Organic Electron.*, vol. 26, pp. 371–379, Nov. 2015.

[18] H. Marien, M. Steyaert, E. van Veenendaal, and P. Heremans, "Analog techniques for reliable organic circuit design on foil applied to an 18 dB single-stage differential amplifier," *Organic Electron.*, vol. 11, no. 8, pp. 1357–1362, Aug. 2010.

[19] A. C. Hübler, M. Bellmann, G. C. Schmidt, S. Zimmermann, A. Gerlach, and C. Haentjes, "Fully mass printed loudspeakers on paper," *Organic Electron.*, vol. 13, no. 11, pp. 2290–2295, Nov. 2012.

[20] G. C. Schmidt, D. Höft, K. Haase, M. Bellmann, B. Kheradmand-Boroujeni, T. Hassinen, H. Sandberg, F. Ellinger, and A. C. Hübler, "Fully printed flexible audio system on the basis of low-voltage polymeric organic field effect transistors with three layer dielectric," *J. Polym. Sci. B, Polym. Phys.*, vol. 53, no. 20, pp. 1409–1415, Oct. 2015.

[21] B. Kheradmand-Boroujeni, G. C. Schmidt, D. Höft, R. Shabanpour, C. Perumal, T. Meister, K. Ishida, C. Carta, A. C. Hübler, and F. Ellinger, "Analog characteristics of fully printed flexible organic transistors fabricated with low-cost mass-printing techniques," *IEEE Trans. Electron Devices*, vol. 61, no. 5, pp. 1423–1430, May 2014.

[22] L. F. Brown and D. L. Carlson, "Ultrasound transducer models for piezoelectric polymer films," *IEEE Trans. Ultrason., Ferroelect., Freq. Control*, vol. 36, no. 3, pp. 313–318, May 1989.

[23] R. S. Dahiya, M. Valle, and L. Lorenzelli, "SPICE model for lossy piezoelectric polymers," *IEEE Trans. Ultrason., Ferroelect., Freq. Control*, vol. 56, no. 2, pp. 387–395, Feb. 2009.

Bahman Kheradmand-Boroujeni received the Ph.D. degree in microsystems and microelectronics from École Polytechnique Fédérale de Lausanne, Lausanne, Switzerland.

He is currently a Scientific Employee with the Center for Advancing Electronics Dresden (cfaed), and the Chair for Circuit Design and Network Theory, Technische Universität Dresden, Dresden, Germany, working on organic/polymeric devices, circuits, and applications.

Georg Cornelius Schmidt received the Diploma degree in microtechnologies and mechatronics and the Ph.D. (Dr. Ing.) degree from Technische Universität Chemnitz, Chemnitz, Germany.

He is currently a Scientific Staff Member with the Institute for Print and Media Technology, Chemnitz.

Daniel Höft received the Dipl.Ing. degree in microtechnologies and mechatronics from Technische Universität Chemnitz, Chemnitz, Germany.

He is currently a Scientific Staff Member with the Institute for Print and Media Technology, Chemnitz.

Maxi Bellmann received a Master's degree in print- and media technology from Technische Universität Chemnitz, Chemnitz, Germany. She is currently working toward the Ph.D. degree as Scientific Staff Member of the Institute for Print and Media Technology, Chemnitz.

Katherina Haase received the M.Sc. degree in media production from Technische Universität Chemnitz, Chemnitz, Germany and the M.Sc. degree in printing and media technology from Manipal University, Manipal, India.

She is currently a Scientific Staff Member of the Institute for Print and Media Technology, Chemnitz.

Koichi Ishida (S'00–M'06) received the Ph.D degree in electronics engineering from the University of Tokyo, Tokyo, Japan, in 2005.

He has been with the Chair for Circuit Design and Network Theory, Dresden University of Technology, Dresden, Germany, since 2012.

Reza Shabanpour received the M.Sc. degree in electronic engineering from the University of Sheffield, Sheffield, U.K., in 2010. He is currently working toward the Ph.D. degree with the Chair for Circuit Design and Network Theory, Technische Universität Dresden, Dresden, Germany.

Tilo Meister (S'07–M'13) received the Diploma degree in electrical engineering and the Ph.D. (Dr. Ing.) degree from the Technische Universität Dresden, Dresden, Germany, in 2006 and 2012, respectively.

He is currently a Researcher with the Chair for Circuit Design and Network Theory, Dresden.

Corrado Carta (S'01–M'06) received the Ph.D. degree from the Swiss Federal Institute of Technology Zurich, Zurich, Switzerland, in 2006.

He is currently with the Technische Universität Dresden, Dresden, Germany, where he is leading the millimeter-wave IC design group and the beyond-Moore electronics group.

Pol Ghesquiere received the Dipl. Ing. degree in chemical engineering from the University KU Leuven, Leuven, Belgium.

He is currently a Senior Key Expert Engineer with the Corporate Technology Department of Siemens in Munich, Germany.

Arved C. Hübler received the Ph.D. in engineering from Hochschule der Künste Berlin, Berlin, Germany.

He was a Chief Technology Manager at Bertelsmann AG, Gütersloh, Germany. Since 1997, he has held the Professorship with Print Media Technology, Chemnitz University of Technology, Chemnitz, Germany.

Frank Ellinger (S'97–M'01–SM'06) received the Dr. sc. techn. habil. and Dipl.Betriebswissenschaften degrees from the University of Ulm, Ulm, Germany, and ETH Zürich, Zürich, Switzerland.

He has been a Full Professor and the Head of the Chair for Circuit Design and Network Theory, Technische Universität Dresden, Dresden, Germany, since 2006.